Inorganic Chemistry

Article

pubs.acs.org/IC

Synthesis and Characterization of Multinuclear Manganese-Containing Tungstosilicates

Rami Al-Oweini,[†] Bassem S. Bassil,[†] Jochen Friedl,[‡,§] Veronika Kottisch,[†] Masooma Ibrahim,[†,▽] Marie Asano,[†] Bineta Keita,[∥] Ghenadie Novitchi,[⊥] Yanhua Lan,[¶] Annie Powell,[¶,▼] Ulrich Stimming,[‡,§,□] and Ulrich Kortz*[,†]

[†]School of Engineering and Science, Jacobs University, P.O. Box 750561, 28725 Bremen, Germany

[‡]TUM CREATE, 1 CREATE Way, CREATE Tower, Singapore 138602, Singapore

[§]Department of Physics E19, Technische Universität München, James-Franck Str. 1, 85748 Garching, Germany

[∥]Laboratoire de Chimie Physique, Groupe d'Electrochimie et de Photoélectrochimie, UMR 8000, CNRS, Université Paris-Sud, Bâtiment 350, 91405 Orsay Cedex, France

[⊥]Laboratoire National des Champs Magnétiques Intenses, CNRS, 25 rue des Martyrs, 38042 Grenoble Cedex 9, France

[¶]Institut für Anorganische Chemie, Karlsruher Institut für Technologie (KIT), Engesserstrasse 15 Geb. 30.45, 76131 Karlsruhe, Germany

[□]Institute for Advanced Study (IAS) of the Technische Universität München, Lichtenbergstr. 2a, 85748 Garching, Germany

[▼]Institute of Nanotechnology, Karlsruhe Institute of Technology, P.O. Box 3640, 76021 Karlsruhe, Germany

Supporting Information

ABSTRACT: The five manganese-containing, Keggin-based tungstosilicates $[Mn^{II}_3(OH)_3(H_2O)_3(A\text{-}\alpha\text{-}SiW_9O_{34})]^{7-}$ (**1**), $[Mn^{III}_3(OH)_3(H_2O)_3(A\text{-}\alpha\text{-}SiW_9O_{34})]^{4-}$ (**2**), $[Mn^{III}_3(OH)_3(H_2O)_3(A\text{-}\beta\text{-}SiW_9O_{34})]^{4-}$ (**3**), $[Mn^{III}_3Mn^{IV}O_3(CH_3COO)_3(A\text{-}\alpha\text{-}SiW_9O_{34})]^{6-}$ (**4**), and $[Mn^{III}_3Mn^{IV}O_3(CH_3COO)_3(A\text{-}\beta\text{-}SiW_9O_{34})]^{6-}$ (**5**) were synthesized in aqueous medium by interaction of $[A\text{-}\alpha\text{-}SiW_9O_{34}]^{10-}$ or $[A\text{-}\beta\text{-}SiW_9O_{34}H]^{9-}$ with either $MnCl_2$ (**1**) or $[Mn^{III}_8Mn^{IV}_4O_{12}(CH_3COO)_{16}(H_2O)_4]$ (**2**–**5**) under carefully adjusted reaction conditions. The obtained salts of these polyanions were analyzed in the solid state by single-crystal X-ray diffraction, IR spectroscopy, and thermogravimetric analysis. The salts of polyanions **1**, **2**, and **4** were further characterized in the solid state by magnetic studies, as well as in solution by electrochemistry.

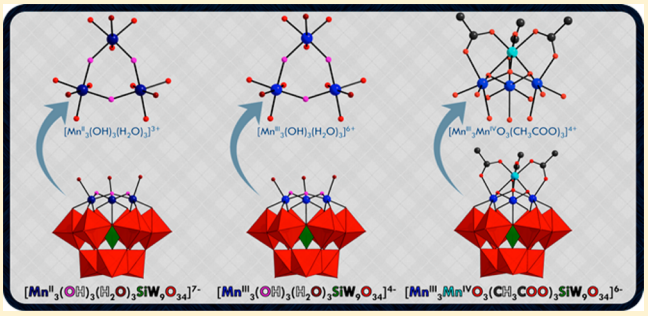

INTRODUCTION

Polyoxometalates (POMs) are inorganic, discrete, and nanosized cage complexes[1] with great prospects in the designing of diverse devices in the areas of catalysis,[2] magnetism,[3] nanostructured material science,[4] and medicine.[5] POMs are typically synthesized following polycondensation reactions (usually in acidic aqueous solution) of simple oxoanions of early transition metals in high oxidation states. The formation mechanism of POMs, commonly identified as "self-assembly," remains not well-understood;[6] however, it is affected by several reaction conditions, such as the ratio of reactants, pH, temperature, and reaction time, among others.[1a,d] Consequently, controlled synthetic routes allow for a rational design of tailored POM assemblies with a variety of shape, size, and complexity.[1,7]

The Keggin and Wells–Dawson-type polyanions are of high interest in the synthesis of transition metal-containing POMs, due to their ability to form stable lacunary derivatives via loss of one or more WO_6 units.[1a] These lacunary precursors can therefore be viewed as inorganic polydentate ligands, with vacant sites containing terminal and basic oxygens that can coordinate to electrophilic centers, particularly transition metal ions.[8] With respect to manganese-containing POMs, a considerable number of structures is reported in the literature,[8a−c,9] whereby $[Mn_{19}(OH)_{12}(SiW_{10}O_{37})_6]^{34-}$,[8c] which is synthesized by a one-pot reaction of $MnCl_2{\cdot}4H_2O$ with $[A\text{-}\alpha\text{-}SiW_9O_{34}]^{10-}$, contains a very large, discrete multinuclear manganese–oxo cluster encapsulated by a tungstosilicate framework. A comprehensive literature survey of manganese-containing polyoxotungstates is shown in Table 1.

Lacunary POMs are also known to react with preformed multinuclear 3d transition metal-based coordination complexes, leading to products that may not be formed using simple metal

Received: February 23, 2014
Published: May 19, 2014

   dx.doi.org/10.1021/ic500425c | Inorg. Chem. 2014, 53, 5663−5673

Table 1. Survey of Known Mn-Substituted Polyoxotungstates

polyanion	Mn^{n+a}	reference
$[Mn^{II}(H_2O)_2(SiW_{10}O_{35})_2]^{10-}$	1	Bassil, Kortz et al. 2006[9d]
$[Mn^{II}(OH_2)AlW_{11}O_{39}]^{7-}$, $[Mn^{III}(OH_2)AlW_{11}O_{39}]^{6-}$, $[Mn^{IV}(OH_2)AlW_{11}O_{39}]^{5-}$	1	Hill, Weinstock et al. 2001[35]
$[Mn^{II}(Br)(P_2W_{17}O_{61})]^{7-}$	1	Neumann et al. 2006[36]
$[Mn^{II}Mn^{III}(OH)(H_2O)SiW_{10}O_{37}]^{6-}$	2	Patzke et al. 2013[37]
$[\{Mn^{II}(H_2O)_4\}_2K_3\{WO_2(H_2O)_2\}_2\{WO(H_2O)\}_3(P_2W_{12}O_{48})_3]^{19-}$	2	Wang et al. 2009[38]
$[Mn^{II}_2(H_2O)_2WO(H_2O)(AsW_9O_{33})_2]^{10-}$	2	Kortz et al. 2001[8a]
$[Mn^{II}_2Na_2(PW_9O_{34})_2]^{12-}$	2	Weinstock, Hill et al. 2005[39]
$[(Mn^{II}SiW_{11}O_{38}OH)_3]^{15-}$	3	Kortz, Matta 2001[9b]
$[Mn^{II}_3(H_2O)_3SiW_9O_{37}]^{10-}$	3	Pope et al. 1992[20]
$[Mn^{II}_3(H_2O)_3(AsW_9O_{33})_2]^{12-}$	3	Mialane, Hervé et al. 2001[40]
$[Mn^{III}_3(H_2O)_5(PW_9O_{34})_2]^{9-}$	3	Al-Oweini, Kortz et al. 2013[9l]
$[Mn^{III}_3(OH)_3(H_2O)_3SiW_9O_{34}]^{4-}$	3	Shevchenko et al. 2013[21]
$[Mn^{II}_4(H_2O)_2(PW_9O_{34})_2]^{10-}$	4	Coronado et al. 1993[33]
$[Mn^{II}_3Mn^{III}(H_2O)_2(PW_9O_{34})_2]^{9-}$, $[Mn^{II}Mn^{III}_3(OH)_2(PW_9O_{34})_2]^{9-}$	4	Pope et al. 1996[25b]
$[Mn^{II}_4(H_2O)_2(XW_9O_{34})_2]^{12-}$ (X = Si, Ge)	4	Kortz et al. 2000,[9a] 2004[8b]
$[Mn^{II}_4(H_2O)_2(P_2W_{15}O_{56})_2]^{16-}$	4	Coronado et al. 1994[41]
$[Mn^{II}_4(H_2O)_{16}P_8W_{48}O_{184}]^{32-}$	4	Bassil, Kortz et al. 2010[9h]
$[\{Mn^{II}_2(SiW_{10}O_{36})(OH)_2(N_3)_{0.5}(H_2O)_{0.5}\}_2(N_3)]^{10-}$	4	Mialane, Sécheresse et al. 2006[42]
$[Mn^{II}_4O_3(Ac)_3(P_2W_{15}O_{56})]^{8-}$	4	Hill, Kögerler et al. 2010[10d]
$[(Mn^{II}_2GeW_{10}O_{38})_3]^{18-}$	6	Cronin et al. 2009[43]
$[((Mn^{II}OH_2)Mn^{II}_2GeW_9O_{34})_2(GeW_6O_{26})]^{18-}$	6	Xu et al. 2010[44]
$[\{(Mn^{III}_4Mn^{II}_2O_4(H_2O)_4)(GeW_9O_{34})_2\}]^{12-}$, $[\{(Mn^{III}_4Mn^{II}_2O_4(H_2O)_4)(SiW_9O_{34})_2\}]^{12-}$	6	Cronin et al. 2008[9e]
$[Mn^{II}_6O_2(H_2O)_4(SiW_8O_{31})(SiW_9O_{34})(SiW_{10}O_{36})]^{18-}$	6	Cronin et al. 2011[45]
$[\{Mn^{II}(H_2O)_2\}\{Mn^{II}_3(H_2O)(SiW_9O_{33}(OH))(SiW_8O_{30}(OH))\}_2]^{22-}$	7	Niu et al. 2011[46]
$[\{Mn^{II}(H_2O)_2\}\{Mn^{II}_3(H_2O)(GeW_9O_{33}(OH))(GeW_8O_{30}(OH))\}_2]^{22-}$	7	Nsouli, Kortz et al. 2009[9g]
$[Mn^{II}_7O_6(H_2O)_6(P_2W_{15}O_{56})_2]^{14-}$	7	Fang, Kögerler et al. 2012[47]
$[Mn^{II}_2\{Mn^{II}_3(H_2O)(SiW_9O_{34})(SiW_6O_{26})\}_2]^{22-}$	8	Cronin et al. 2010[9i]
$[\{Mn^{III}_3Mn^{IV}_4O_4(OH)_2(OH_2)\}_2(W_6O_{22})(H_2W_8O_{32})_2(H_4W_{13}O_{46})_2]^{26-}$	14	Fang, Luban 2011[48]
$[Mn^{III}_{13}Mn^{II}O_{12}(PO_4)_4(PW_9O_{34})_4]^{31-}$	14	Wang, Clérac et al. 2009[10c]
$[Mn^{II}_{19}(OH)_{12}(SiW_{10}O_{37})_6]^{34-}$	19	Bassil, Kortz et al. 2011[8c]
$[\{(Mn^{III}_4P_2W_{14}O_{60})(Mn^{III}_3P_2W_{15}O_{58})_2\}_4(P_8W_{48}O_{184})]^{144-}$	40	Fang, Kögerler et al. 2011[10e]

[a]The number of Mn^{n+} ions incorporated in the polyanion structure.

salts. This methodology has attracted increasing interest, and to date several polyanions synthesized accordingly are known.[9e,10] In particular, the well-known dodecanuclear, high-valent manganese complex $[Mn^{III}_8Mn^{IV}_4O_{12}(CH_3COO)_{16}(H_2O)_4]$ (**Mn_{12}**),[11] which was shown to exhibit single molecule magnet behavior,[12] has been mostly used. Our group has also just recently reported on the interaction of **Mn_{12}** with the trilacunary Keggin ion $[A\text{-}\alpha\text{-}PW_9O_{34}]^{9-}$, resulting in a manganese(III)-containing, sandwich-type tungstophosphate $[Mn^{III}_3(H_2O)_5(A\text{-}\alpha\text{-}PW_9O_{34})_2]^{9-}$.[9l]

Here we report on the interaction of the two trilacunary 9-tungstosilicate precursors $[A\text{-}\alpha\text{-}SiW_9O_{34}]^{10-}$ and $[A\text{-}\beta\text{-}SiW_9O_{34}H]^{9-}$ with either $MnCl_2{\cdot}4H_2O$ or **Mn_{12}** in aqueous medium under various synthetic conditions.

EXPERIMENTAL SECTION

Synthesis. The hydrated sodium and potassium salts of the trilacunary 9-tungstosilicate precursor $Na_{10}[A\text{-}\alpha\text{-}SiW_9O_{34}]{\cdot}14H_2O$, $Na_9[A\text{-}\beta\text{-}SiW_9O_{34}H]{\cdot}23H_2O$, and $K_{10}[A\text{-}\alpha\text{-}SiW_9O_{34}]{\cdot}24H_2O$ were synthesized following published procedures.[13] The synthesis of the dodecanuclear coordination complex $[Mn^{III}_8Mn^{IV}_4O_{12}(CH_3COO)_{16}(H_2O)_4]{\cdot}2CH_3COOH{\cdot}4H_2O$ (**Mn_{12}**) was carried out according to the reported method by Lis.[11] The identity of the starting materials was confirmed in the solid by infrared (IR) spectroscopy as well as by X-ray diffraction measurements for **Mn_{12}**. All other reagents were used as purchased without further purification.

$Na_{2.5}K_{4.5}[Mn^{II}_3(OH)_3(H_2O)_3(A\text{-}\alpha\text{-}SiW_9O_{34})]{\cdot}15H_2O$ (1a). A sample of $MnCl_2{\cdot}4H_2O$ (0.125 g, 0.63 mmol) was dissolved in 20 mL of water, and then solid $K_{10}[A\text{-}\alpha\text{-}SiW_9O_{34}]{\cdot}24H_2O$ (0.52 g, 0.20 mmol) was added and stirred until complete dissolution. The pH of the mixture was then adjusted to 8 via NaOH solution (4 M), followed by stirring at 50 °C for 30 min. The mixture was then allowed to cool to room temperature and filtered. Slow evaporation of the filtrate at room temperature led to the formation of dark-gray crystals of **1a** within two weeks (yield based on W = 0.08 g, 15%). The structure of polyanion **1** is shown in Figure 1 (see also Supporting Information, Figure S1). IR (cm^{-1}): 995 (m), 970 (sh), 949 (m), 913 (sh), 897 (s), 769 (s), 709 (m), 539 (w), see Figure 2. Elemental analysis for **1a** (M_w 3000.3 g/mol) % calc. (found): K 5.8 (5.7), Mn 5.5 (5.4), Si 0.9 (1.2), W 55.1 (55.2).

$K_4[Mn^{III}_3(OH)_3(H_2O)_3(A\text{-}\alpha\text{-}SiW_9O_{34})]{\cdot}10H_2O$ (2a) and $NaK_3[Mn^{III}_3(OH)_3(H_2O)_3(A\text{-}\beta\text{-}SiW_9O_{34})]{\cdot}10H_2O$ (3a). A sample of

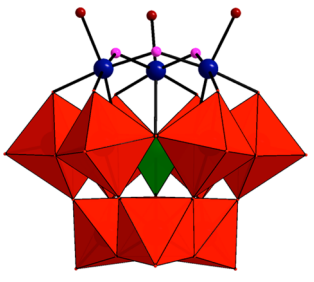

Figure 1. Combined polyhedral/ball-and-stick representation of **1**. Color code, balls: manganese(II) (dark-blue), hydroxide (pink); terminal waters (dark-red); polyhedra: SiO_4 (green), WO_6 (red).

dx.doi.org/10.1021/ic500425c | Inorg. Chem. 2014, 53, 5663−5673

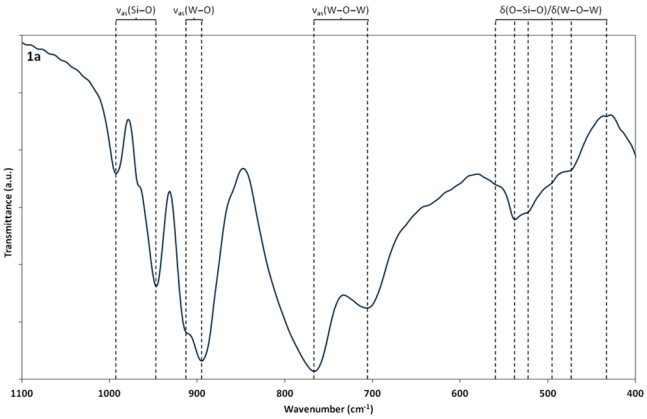

Figure 2. FTIR spectrum of **1a**.

$[Mn^{III}_8Mn^{IV}_4O_{12}(CH_3COO)_{16}(H_2O)_4]\cdot 2CH_3COOH\cdot 4H_2O$ (**Mn_{12}**) (0.21 g, 0.10 mmol) was suspended for a few seconds in 20 mL of water, and then solid $Na_{10}[A\text{-}\alpha\text{-}SiW_9O_{34}]\cdot 14H_2O$ for **2a** or $Na_9[A\text{-}\beta\text{-}SiW_9O_{34}H]\cdot 23H_2O$ for **3a** (0.55 g, 0.20 mmol) was quickly added. The pH was adjusted to 4 via HCl solution (1 M), and the mixture was stirred for 1 h at room temperature. Some unreacted starting material, mainly **Mn_{12}**, was filtered off at this stage, followed by the addition of 1 mL of KCl solution (1 M) to the filtrate. Slow evaporation of the solution at room temperature led to the formation of brown crystals within two weeks. Yield based on W = 0.28 g (48%) and 0.25 g (43%) for **2a** and **3a**, respectively. The structures of polyanions **2** and **3** are shown in Figure 3 (see also Supporting Information, Figure S2). IR for

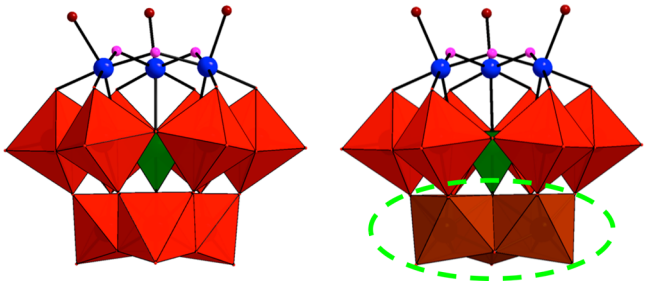

Figure 3. Combined polyhedral/ball-and-stick representation of **2** (left) and **3** (right). Color code, balls: manganese(III) (blue), hydroxide (pink); terminal waters (dark-red); polyhedra: SiO_4 (green), WO_6 (red). The rotated triad of **3** is shown in dark-red and is highlighted in bright green.

2a (cm^{-1}): 1075 (w), 1039 (w), 1002 (w), 979 (m), 963 (m), 927 (s), 772 (s), 706 (m), 653 (w), 592 (w), 522 (m), 496 (sh), 474 (w), 436 (w), see Figure 4. Elemental analysis for **2a** (M_w 2833.2 g/mol) % calc. (found): K 5.5 (5.5), Mn 5.8 (5.7), Si 1.0 (1.1), W 58.4 (57.1). IR for **3a** (cm^{-1}): 1100 (w), 999 (m), 958 (m), 912 (s), 851 (sh), 809 (s), 774 (s), 711 (s), 598 (w), 526 (m), 479 (sh), see Figure 4.

$Na_{3.5}K_{2.5}[Mn^{III}_3Mn^{IV}O_3(CH_3COO)_3(A\text{-}\alpha\text{-}SiW_9O_{34})]\cdot 20H_2O\cdot NaCH_3COO\cdot 0.5KCH_3COO$ (4a) and $Na_{3.5}K_{2.5}[Mn^{III}_3Mn^{IV}O_3(CH_3COO)_3(A\text{-}\beta\text{-}SiW_9O_{34})]\cdot 19H_2O\cdot NaCH_3COO\cdot 0.5KCH_3COO$ (5a). A sample of $[Mn^{III}_8Mn^{IV}_4O_{12}(CH_3COO)_{16}(H_2O)_4]\cdot 2CH_3COOH\cdot 4H_2O$ (**Mn_{12}**) (0.42 g, 0.20 mmol) was suspended for a few seconds in 20 mL of sodium acetate buffer solution (1 M, pH 6), and then solid $Na_{10}[A\text{-}\alpha\text{-}SiW_9O_{34}]\cdot 14H_2O$ for **4a** or $Na_9[A\text{-}\beta\text{-}SiW_9O_{34}H]\cdot 23H_2O$ for **5a** (0.55 g, 0.20 mmol) was quickly added. The mixture was then stirred for 1 h at room temperature. Some unreacted starting material, mainly **Mn_{12}**, was filtered off at this stage, followed by the addition of 1 mL of KCl solution (1 M) to the filtrate. Slow evaporation of the solution at room temperature led to the formation of dark-brown crystals within two weeks. Yield based on W = 0.33 g (52%) and 0.31 g (49%) for **4a** and **5a**, respectively. The structures of

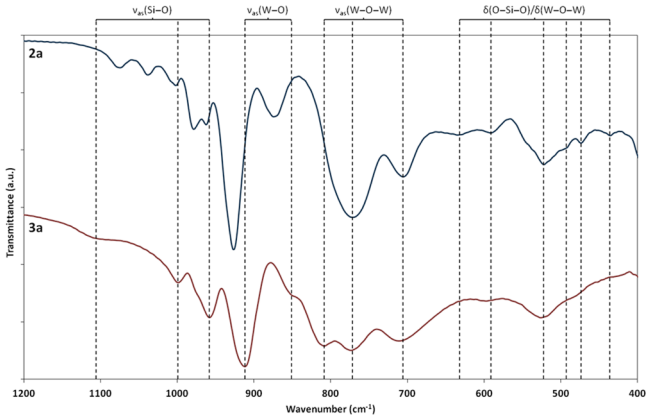

Figure 4. FTIR spectra of **2a** (upper) and **3a** (lower).

polyanions **4** and **5** are shown in Figure 5 (see also Supporting Information, Figure S3). IR for **4a** (cm^{-1}): 1672 (m), 1575 (m), 1545

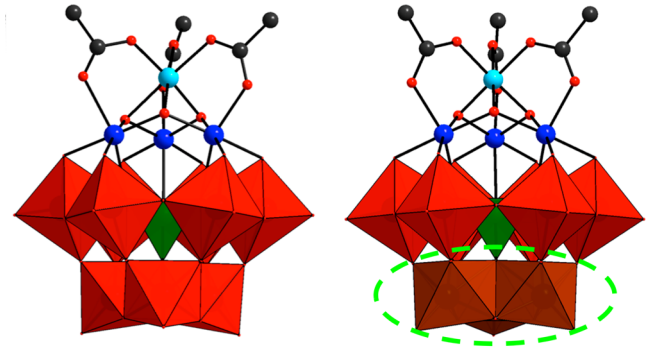

Figure 5. Combined polyhedral/ball-and-stick representation of **4** (left) and **5** (right). Color code, balls: manganese(III) (blue), manganese(IV) (light-blue), oxygen (red); carbon (dark-gray); polyhedra: SiO_4 (green), WO_6 (red). The rotated triad of **5a** is shown in dark-red and is highlighted in bright green.

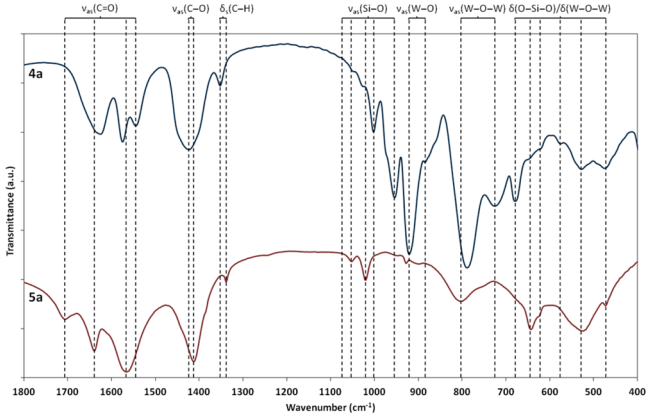

Figure 6. FTIR spectra of **4a** (upper) and **5a** (lower).

(m), 1424 (s), 1352 (w), 1002 (w), 954 (m), 921 (s), 885 (sh), 789 (s), 726 (m), 679 (m), 576 (w), 529 (w), 475 (w), see Figure 6. Elemental analysis for **4a** (M_w 3341.3 g/mol) % calc. (found): C 3.2 (2.6), H 1.6 (1.3), Na 3.1 (3.1), K 3.5 (3.7), Mn 6.6 (6.5), Si 0.9 (0.9), W 49.5 (46.7). IR for **5a** (cm^{-1}): 1706 (m), 1639 (m), 1566 (s), 1412 (s), 1339 (w), 1052 (w), 1021 (m), 927 (w), 804 (m), 643 (m), 524 (m), 473 (w), see Figure 6.

dx.doi.org/10.1021/ic500425c | Inorg. Chem. 2014, 53, 5663−5673

Instrumentation. IR spectra were recorded on a Nicolet Avatar 370 FT-IR spectrophotometer using KBr pellets. The following abbreviations were used to assign the peak intensities: w = weak; m = medium; s = strong; sh = shoulder. Thermogravimetric analysis (TGA) was carried out on a TA Instruments SDT Q600 thermobalance with a 100 mL/min flow of nitrogen; the temperature was ramped from 20 to 800 °C at a rate of 5 °C/min. Elemental analysis was performed by CNRS, Service Central d'Analyze, Solaize, France.

X-ray Crystallography. Single crystals of **1a**−**5a** were mounted on a Hampton cryoloop in light oil for data collection at −100 °C. Indexing and data collection were performed on a Bruker D8 SMART APEX II CCD diffractometer with kappa geometry and Mo Kα radiation (graphite monochromator, λ = 0.710 73 Å). Data integration was performed using *SAINT*.[14] Routine Lorentz and polarization corrections were applied. Multiscan absorption corrections were performed using *SADABS*.[15] Direct methods (*SHELXS97*) successfully located the tungsten atoms, and successive Fourier syntheses (*SHELXL97*) revealed the remaining atoms.[15] Refinements were done using full-matrix least-squares against F^2 on all data. In the final refinement, the W, Mn, Si, K, and Na atoms were refined anisotropically; the O and C atoms as well as the disordered K and Na countercations were refined isotropically. The hydrogen atoms of the acetate groups in **4a** and **5a** were placed in calculated positions and then refined using a riding model. The complete X-ray crystallographic data (CIF format) and a summary of the crystallographic data are in Supporting Information.

Electrochemistry. The electrochemical setup was either an EG&G 273 A driven by a personal computer (PC) with the M270 software or a Bio-Logic SP-300 controlled by a PC with the EC-Lab software. The working electrode was a pretreated indium tin oxide (ITO) electrode in the case of **2** and **4**,[16] or a polished glassy carbon electrode for **1**. Potentials were measured against a saturated calomel reference electrode (SCE). The counter electrode was a platinum gauze of large surface area. Pure water from a RiOs 8 unit followed by a Millipore-Q Academic purification set was used throughout. The solutions were deaerated thoroughly for at least 30 min with pure argon and kept under a positive pressure of this gas during the experiments. The composition of the aqueous medium was 1 M $LiCH_3COO$ + CH_3COOH (pH 5).

Magnetic Studies. Magnetic susceptibility data (1.8−300 K) were collected on powdered samples using a SQUID magnetometer (Quantum Design MPMS-XL), applying magnetic fields of 0.1 T. All data were corrected for the contribution of the sample holder and the diamagnetism of the samples estimated from Pascal's constants.[17] Magnetic data analyses were carried out with the MAGPACK program package by calculations of energy levels associated with the spin Hamiltonians presented in the text.[18]

RESULTS AND DISCUSSION

Synthesis and Structure. The interaction of the potassium salt of $[A\text{-}\alpha\text{-}SiW_9O_{34}]^{10-}$ with manganese(II) ions in aqueous, basic medium (pH 8) and under mild heating resulted in the formation of the trimanganese-containing silicotungstate $[Mn^{II}_3(OH)_3(H_2O)_3(A\text{-}\alpha\text{-}SiW_9O_{34})]^{7-}$ (**1**), which crystallizes as a hydrated mixed sodium−potassium salt, $Na_{2.5}K_{4.5}[Mn^{II}_3(OH)_3(H_2O)_3(A\text{-}\alpha\text{-}SiW_9O_{34})]\cdot 15H_2O$ (**1a**), in the rhombohedral space group $R\bar{3}$. Polyanion **1** can also be synthesized by using the sodium salt of $[A\text{-}\alpha\text{-}SiW_9O_{34}]^{10-}$ and room temperature conditions, but in both cases yield and purity were lower. Single-crystal XRD measurements on **1a** revealed the structure of polyanion **1**, comprising a $\{A\text{-}\alpha\text{-}SiW_9O_{34}\}$ unit with three incorporated Mn^{II} ions, resulting in a plenary Keggin assembly with C_{3v} symmetry (Figure 1). The three manganese centers are connected to each other by hydroxo bridges, and each Mn^{II} ion has a terminal aqua ligand, which were identified by bond valence sum (BVS) calculations (Supporting Information, Table S2).[19] TGA was also performed on **1a** and resulted in 15 crystal waters (Supporting Information, Figure S4), fully consistent with elemental analysis.

As polyanion **1** could be synthesized by direct reaction of manganese(II) chloride with the trilacunary POM precursor, we also tried to prepare its Mn^{III}-analogue by using the same approach but without success. Therefore, we decided to test other water-soluble, high-valent manganese sources, including multinuclear coordination complexes. Consequently, reaction of the dodecanuclear, mixed-valent coordination complex $\mathbf{Mn_{12}}$ with $Na_{10}[A\text{-}\alpha\text{-}SiW_9O_{34}]$ in mildly acidic aqueous medium (pH ≈ 4) and in a molar ratio of 1:2 at room temperature resulted in the formation of the manganese(III)-containing, Keggin-based tungstosilicate $[Mn^{III}_3(OH)_3(H_2O)_3(A\text{-}\alpha\text{-}SiW_9O_{34})]^{4-}$ (**2**) as a hydrated potassium salt, $K_4[Mn^{III}_3(OH)_3(H_2O)_3(A\text{-}\alpha\text{-}SiW_9O_{34})]\cdot 10H_2O$ (**2a**), which crystallized in the monoclinic space group $P2_1/n$. Polyanions **2** and **1** are isostructural, with the only difference that the former contains three manganese(III) ions and the latter three manganese(II) ions (Figure 3). The BVS values for the manganese ions in **2** were found to be 3.08, 3.17, and 3.14 for Mn1, Mn2, and Mn3, respectively, confirming the assigned +3 oxidation states (Supporting Information, Table S3), and BVS also indicated that the μ_2-O bridges linking the three Mn ions are monoprotonated.[19,20]

The β-analogue of polyanion **2** could also be synthesized by reacting $\mathbf{Mn_{12}}$ with the trilacunary β-Keggin precursor $Na_9[A\text{-}\beta\text{-}SiW_9O_{34}H]\cdot 23H_2O$, leading to the target polyanion $[Mn^{III}_3(OH)_3(H_2O)_3(A\text{-}\beta\text{-}SiW_9O_{34})]^{4-}$ (**3**). This compound was isolated as a hydrated mixed sodium−potassium salt $NaK_3[Mn^{III}_3(OH)_3(H_2O)_3(A\text{-}\beta\text{-}SiW_9O_{34})]\cdot 10H_2O$ (**3a**), which crystallized in the monoclinic space group $P2_1/c$. The key difference between **2** and **3** is that the latter has the edge-shared W_3O_{13} triad opposite to the manganese ions rotated by 60°, and thus the structures of the β- versus α-Keggin precursors are retained in **3** and **2**, respectively (Supporting Information, Figure S9), as confirmed by XRD and FTIR measurements (Figure 4). TGA was also performed on **2a** and **3a** (Supporting Information, Figures S5 and S6), and 10 crystal waters were identified for each.

The $\{Mn_3\}$ structural motif in **1** and **2** has been seen already in the mixed-valent manganese(II,III)-containing, Keggin-type tungstosilicate $[Mn^{II}Mn^{III}_2(H_2O)_3SiW_9O_{37}]^{8-}$,[9j] in the manganese(II)-containing $[Mn^{II}_3(H_2O)_3(A\text{-}\alpha\text{-}SiW_9O_{37})]^{10-}$ and its β-analogue $[Mn^{II}_3(H_2O)_3(A\text{-}\beta\text{-}SiW_9O_{37})]^{10-}$, the latter two without crystal structure,[20] and also in the manganese(III)-containing $[Mn^{III}_3(OH)_3(H_2O)_3(A\text{-}\alpha\text{-}SiW_9O_{34})]^{4-}$,[21] which is isostructural with polyanion **2**, but was prepared via a different synthetic route. In this context, we can draw a comparison between the $\{Mn^{II}_3\}$ assembly in **1**, $\{Mn^{II}Mn^{III}_2\}$ in the previously reported polyanion,[9j] and $\{Mn^{III}_3\}$ in **2**. All three polyanions contain the $[A\text{-}\alpha\text{-}SiW_9O_{34}]^{10-}$ trilacunary Keggin fragment with three manganese ions in the vacant sites, being connected via hydroxo bridges, leading to a plenary Keggin-assembly with idealized C_{3v} point group symmetry. As expected, we observed a Jahn−Teller distortion for the octahedrally coordinated, high-spin Mn^{III} ions (d^4 electronic configuration), but not for the high-spin Mn^{II} centers (d^5 electronic configuration). On the basis of XRD, the following Mn−O bond length ranges for the three types of Keggin-type polyanions containing $\{Mn^{II}_3\}$, $\{Mn^{II}Mn^{III}_2\}$, or $\{Mn^{III}_3\}$ units were observed: 1.971(17)−1.997(18), 1.978(9)−2.160(8), and 1.929(10)−1.952(10) Å, respectively, for bridging Mn−OH−Mn bonds, as well as 2.174(22),

dx.doi.org/10.1021/ic500425c | *Inorg. Chem.* 2014, 53, 5663−5673

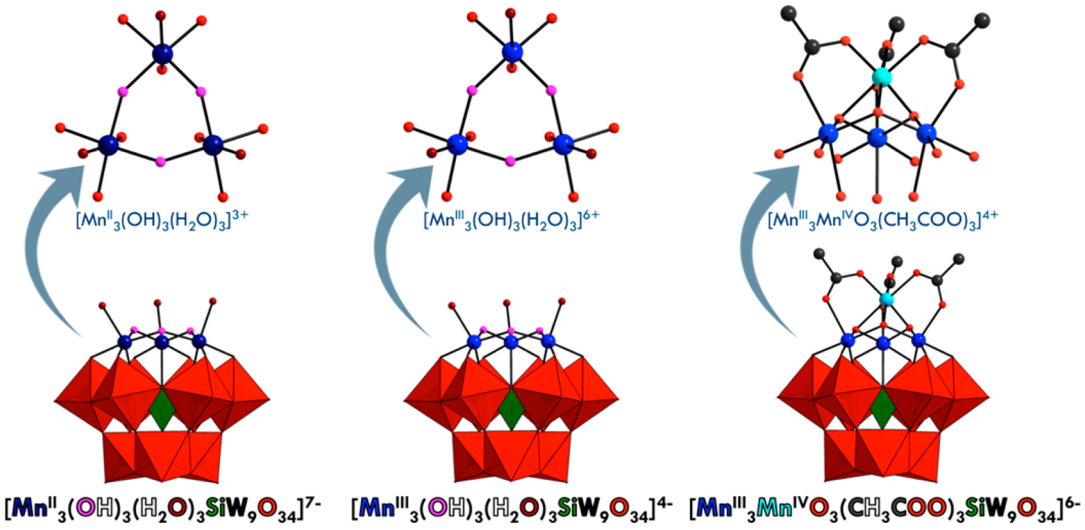

Figure 7. Comparison of the Mn−oxo clusters in polyanions **1** (left), **2** (middle), and **4** (right).

2.160(8), and 2.156(10)−2.197(10) Å, respectively, for terminal Mn−OH_2 bonds (Supporting Information, Tables S3 and S4).

Interestingly, the interaction of $\mathbf{Mn_{12}}$ with $Na_{10}[A\text{-}\alpha\text{-}SiW_9O_{34}]$ in sodium acetate buffer (pH ≈ 6) in a 1:1 molar ratio at room temperature resulted in the formation of the mixed-valent manganese(III/IV)-containing tungstosilicate $[Mn^{III}_3Mn^{IV}O_3(CH_3COO)_3(A\text{-}\alpha\text{-}SiW_9O_{34})]^{6-}$ (**4**), which crystallized as a hydrated mixed sodium−potassium salt $Na_{3.5}K_{2.5}[Mn^{III}_3Mn^{IV}O_3(CH_3COO)_3(A\text{-}\alpha\text{-}SiW_9O_{34})]\cdot 20H_2O$ (**4a**) in the triclinic space group $P\bar{1}$. The defective-cubane-shaped, mixed-valent tetra-manganese core $[Mn^{III}_3Mn^{IV}O_3(CH_3COO)_3]^{4+}$ in **4** is stabilized by a trivacant $[A\text{-}\alpha\text{-}SiW_9O_{34}]^{10-}$ Keggin unit, resulting in an overall 6− charge for the polyanion. Alternatively, **4** could be viewed as a $\{Mn^{III}_3SiW_9\}$ Keggin assembly being capped by a $\{Mn^{IV}(CH_3COO)_3\}$ group, resulting in a structure with idealized C_{3v} point group symmetry (Figure 5). The oxidation state of the manganese centers was also confirmed by BVS (Supporting Information, Table S4).[19] The three acetate ligands in **4** originate from the $\mathbf{Mn_{12}}$ precursor or the synthesis medium, which was 1 M acetate buffer. The β-analogue of polyanion **4** could also be synthesized, by performing the reaction with the trilacunary β-Keggin precursor $Na_9[A\text{-}\beta\text{-}SiW_9O_{34}H]\cdot 23H_2O$, resulting in $[Mn^{III}_3Mn^{IV}O_3(CH_3COO)_3(A\text{-}\beta\text{-}SiW_9O_{34})]^{6-}$ (**5**), which crystallized as a hydrated sodium−potassium salt, $Na_{3.5}K_{2.5}[Mn^{III}_3Mn^{IV}O_3(CH_3COO)_3(A\text{-}\beta\text{-}SiW_9O_{34})]\cdot 19H_2O$ (**5a**), in the monoclinic space group $C2/c$. As for polyanions **2** and **3**, the structural similarities between **4** and **5** were confirmed by XRD and FTIR measurements (Figure 6). TGA was also performed on **4a** and **5a** (Supporting Information, Figures S7 and S8), and resulted in 20 and 19 water molecules, respectively. The defective-cubane-shaped, mixed-valent manganese−oxo cluster $[Mn^{III}_3Mn^{IV}O_3(CH_3COO)_3]^{4+}$ almost certainly originates from decomposition of $\mathbf{Mn_{12}}$ during the synthetic procedure and is then stabilized by incorporation into the lacunary polyanion precursor. Such tetra-manganese−oxo cluster has been previously observed in the Wells−Dawson-type polyanion $[Mn^{III}_3Mn^{IV}O_3(CH_3COO)_3(\alpha\text{-}P_2W_{15}O_{56})]^{8-}$,[10d] as well as in other coordination complexes.[22]

In summary, we prepared five novel polyanions **1**−**5**, which can all be viewed as comprising cationic manganese−oxo clusters, such as $[Mn^{II}_3(OH)_3(H_2O)_3]^{3+}$ (in **1**), $[Mn^{III}_3(OH)_3(H_2O)_3]^{6+}$ (in **2** and **3**), and $[Mn^{III}_3Mn^{IV}O_3(CH_3COO)_3]^{4+}$ (in **4** and **5**), respectively, incorporated in a $[A\text{-}SiW_9O_{34}]^{10-}$ Keggin fragment (Figure 7).

Infrared Spectroscopy. The Fourier transform infrared spectra (FTIR) of **1a**−**5a** are shown in Figures 2, 4, and 6, and they show strong and medium bands in the range of 1100−950 cm^{-1}, as well as strong and weak bands in the range of 950−850 cm^{-1}, associated with the antisymmetric stretching vibrations of the Si−O(W) and the terminal W═O bonds, respectively. The medium to strong bands at approximately 820−700 cm^{-1} originate from antisymmetric stretching of the W−O(W) bridges, and weak to medium intensity bands below 650 cm^{-1} correspond to bending vibrations of the central Si−O(W) and the W−O(W) bridges.[4c,e,9l,23,24] Moreover, the FTIR spectra for polyanions **4a** and **5a** also show several medium to strong peaks in the range of 1700−1300 cm^{-1}, which are attributed to vibrations of the bridging acetate groups, stabilizing the mixed-valent manganese(III,IV)−oxo assembly.

Electrochemistry. Polyanions **1**, **2**, and **4** were also studied by cyclic voltammetry (CV) in a pH 5 medium (1 M $LiCH_3COO$ + CH_3COOH). In particular, we assessed the effect of the potential scanning direction and the successive potential cycles on the evolution of the redox characteristics of their Mn and W centers. Electrochemical generation of high-valent manganese center(s) within polyoxotungstates was demonstrated by Pope and co-workers in the 1990s.[20,25] However, in aqueous media, this reaction is often governed by a mixed adsorption−diffusion regime,[9i,k,26] attributed to a concomitant partial thin-film deposition (likely Mn oxides) on the working electrode surface. This electrodeposition process was evidenced for $[\{Mn^{III}(H_2O)\}_3(SbW_9O_{33})_2]^{9-}$ by Keita and co-workers, who resorted to the electrochemical quartz crystal microbalance.[26] Such surface phenomenon could also interfere with the redox behavior of the Mn and W centers. For example, Ammam and co-workers reported for $[Mn_4(H_2O)_2(H_4AsW_{15}O_{56})_2]^{18-}$ a deleterious effect of the electrodeposited film on its W-reduction waves, which became less well-defined and negatively shifted with respect to the

dx.doi.org/10.1021/ic500425c | Inorg. Chem. 2014, 53, 5663−5673

corresponding characteristics obtained with the bare working electrode.[27]

Figure 8A shows the CV of **2** restricted to the quasi-reversible waves relevant to its Mn^{III} and W^{VI} centers at a scan

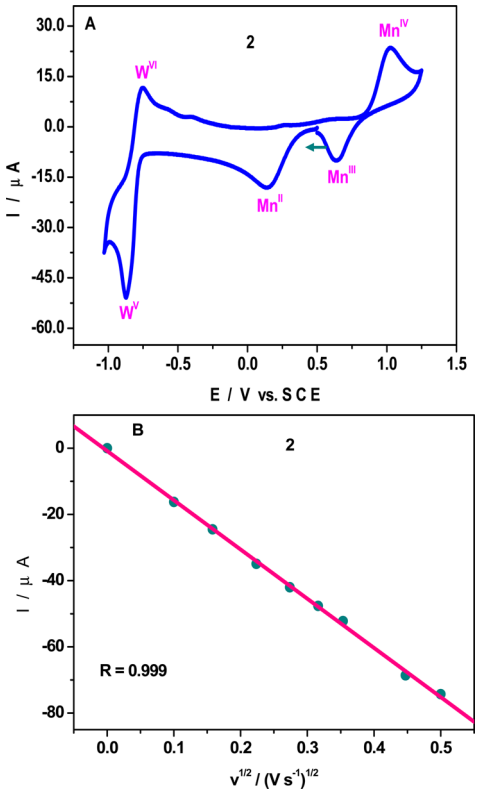

Figure 8. Cyclic voltammograms (CV) of 2×10^{-4} M **2** in a pH 5 medium (1 M $LiCH_3COO$ + CH_3COOH). The scan rate was 100 mV s^{-1}. (A) The CV is restricted to the chemically reversible waves associated with the W and Mn centers. (B) Variation of the cathodic peak current intensity of the W-wave as a function of the square root of the potential scan rate.

rate of 100 mV s^{-1}. When the potential scan is started first toward negative potential values, the pattern exhibits a well-defined wave at +0.145 V versus SCE, attributed to the simultaneous one-electron reduction of the Mn^{III} centers. Whatever the potential scan rate from 250 mV s^{-1} to 10 mV s^{-1}, no splitting of this wave was observed. It is worth noting that the reduction of the Mn^{III} centers within **2** is featured by two separate waves in 0.1 M lutidine buffer (pH 7) as supporting electrolyte.[21] As expected, the W^{VI} reduction wave is located at more negative potential (−0.870 V versus SCE) than that of the Mn^{III} centers. On potential reversal, the two waves located at −0.750 V and +1.020 V versus SCE are associated with the oxidation of the W^{V} and Mn^{II} centers, respectively. The latter is preceded by a low-intensity prewave at ca. +0.630 V versus SCE. These observations feature the stepwise oxidation of Mn^{II} to Mn^{IV}.[9i,k,26] In accordance with previous observations, the resulting Mn^{IV} centers are simultaneously reduced into Mn^{III} at +0.630 V versus SCE. The shape of the CV region for the W centers features the fingerprint voltammetric pattern of the lacunary precursor $[A\text{-}\alpha\text{-}SiW_9O_{34}]^{10-}$. This CV is characterized by a quasi-reversible four-electron reduction wave.[28] The anodic to cathodic peak potential difference of this redox couple (ΔE_p) is ca. 0.120 V at 100 mV s^{-1}. The variation of the W-reduction peak current intensity as a function of the square root of the potential scan rate is shown in Figure 8B. The linearity (R = 0.999) of this curve indicates that this wave is diffusion-controlled. For **2** a good reproducibility was observed in the pH 5 medium for the CV run between +0.650 V and −1 V versus SCE, over a period of several hours, which underscores the stability of **2** in the pH 5 medium and with this potential scanning program. This behavior contrasts with that of the trilacunary precursor $[A\text{-}\alpha\text{-}SiW_9O_{34}]^{10-}$, which undergoes a chemical transformation in aqueous media, ultimately generating $[\alpha\text{-}SiW_{11}O_{39}]^{8-}$.[13a] In contrast, a slow transformation of the CV pattern of **2** was observed upon successive potential cycling in the whole potential domain featuring the quasi-reversible waves of the Mn^{III} and W^{VI} centers (Supporting Information, Figure S10). Especially, the current intensity of the W reduction-wave decreases, and close to this wave a new postwave is observed at −0.950 V versus SCE already in the second cycle. Full characterization of the main compound resulting from this slow conversion of **2** is beyond the scope of the present work. In this context it should be interesting to study the influence of the nature, the pH, and the ionic strength of the supporting electrolyte on such phenomenon. Indeed, Pope and co-workers reported a pH-dependent conversion of a large family of POMs of the type $[SiW_9O_{37}\{M(H_2O)\}_3]^{n-}$ (including β-$[SiW_9O_{37}\{Mn(H_2O)\}_3]^{10-}$) into $[SiW_{11}O_{39}M(H_2O)]^{m-}$.[20] It is worth noting that the successive potential cycles induce a steady cathodic shift of the Mn^{IV} wave, which means that the oxidation process becomes easier. Moreover, the oxidation peak current intensity increases slightly after each follow-up scan. In accordance with previous reports, these observations are ascribed to thin-film deposition on the electrode, with gradual activation of its surface.[9d,h,i,k,l,26]

Figure S11 in the Supporting Information shows that the Mn^{IV} wave is followed by an irreversible oxidation wave at +1.420 V versus SCE, close to the electrolyte discharge limit. On the basis of literature reports, this wave is attributed to the Mn^{V} state.[9d,h,l,29] Reaching this oxidation wave induces a significant decrease of the Mn^{IV} reduction-wave intensity. Such phenomenon was also observed when the explored potential range was restricted to the redox processes of the Mn-centers. Furthermore, the peak-current ratio of the Mn^{V} wave to that of Mn^{IV} increases as the scan rate decreases. It is likely that these processes are, at least partly, due to the modification of the electrode surface during the film electrodeposition with concomitant water electrocatalytic oxidation.[9d,h,l,29]

A comparison of the electrochemical properties of **2** and **4**, under the same conditions, indicates that the redox characteristics of their W^{VI} centers are similar. Considering their overall negative charges, polyanion **2** should be, on a purely electrostatic basis, the easiest to reduce. In general, this behavior is related to other key parameters, such as the acid−base properties of the reduced POMs.[28,30] As expected, the peak current intensities related to the Mn waves are higher for **4** than they are for **2**, as the former contains more Mn centers (Supporting Information, Figure S12). The CV of **4** undergoes also the transformations observed for **2** upon successive potential cycling in the potential domain of its chemically reversible waves (Supporting Information, Figure S12) or when the potential scanning is extended up to the Mn^{V} oxidation wave (Supporting Information, Figure S13).

For both polyanions, it is notable that no inhibition of the different redox centers was observed, whatever the potential domain and the potential scanning programs specified above.

dx.doi.org/10.1021/ic500425c | Inorg. Chem. 2014, 53, 5663−5673

Moreover, steady working electrode activation was observed under certain conditions. This behavior is important for redox or electrocatalytic applications involving the W and/or the Mn centers of these polyanions.

Figure 9A shows the CV of **1** in the same potential range as for **2** in Figure 8A, at a scan rate of 100 mV s^{-1}. A qualitative

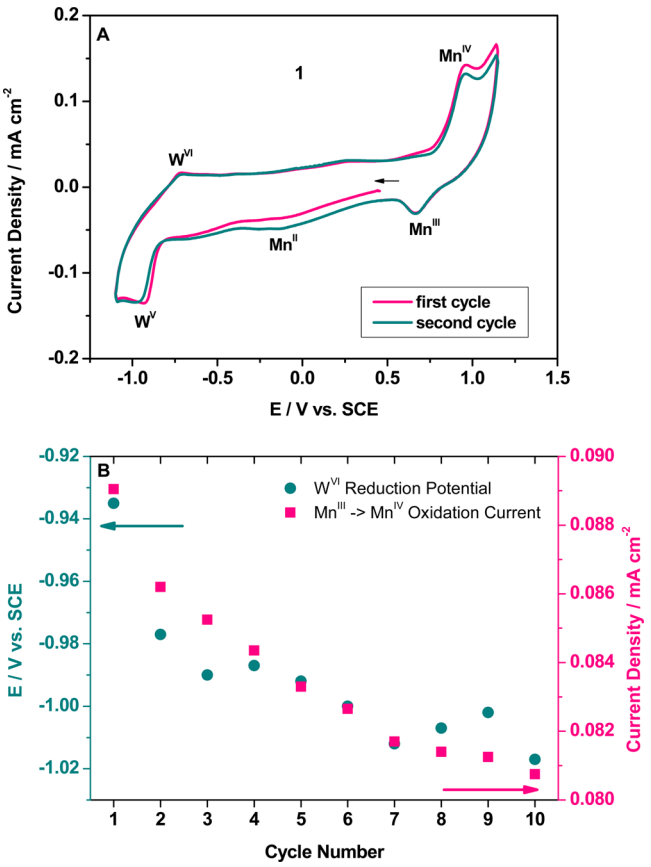

Figure 9. Cyclic voltammograms (CV) of 2×10^{-4} M **1** in a pH 5 medium (1 M $LiCH_3COO + CH_3COOH$). The scan rate was 100 mV s^{-1}. (A) The CV is restricted to the chemically reversible waves associated with the W and Mn centers. (B) Changes induced by successive cycling to 1.15 V vs SCE. The reduction peak for $W^{VI} \rightarrow W^{V}$ shifts to higher potentials (left ordinate), while the current density for the $Mn^{III} \rightarrow Mn^{IV}$ oxidation decreases (right ordinate).

difference to the CVs of **2** and **4** (Supporting Information, Figure S12) is immediately apparent. We attribute this to the fact that **1** contains Mn^{II} centers and not Mn^{III} centers as in **2** and **4**. At open circuit potential the cell rested at 0.45 V versus SCE, a potential at which the Mn^{II} were partially oxidized. Therefore, even in the first cycle, a stepwise Mn^{III} reduction to Mn^{II} was observed at −0.13 V and −0.65 V versus SCE. This reduction behavior contrasts the well-defined, one-step Mn^{III} reduction wave observed for **2** and **4** at +0.145 V versus SCE. At lower potentials the reduction of W^{VI} to W^{V} (−0.93 V vs SCE) followed by reoxidation to W^{VI} (−0.72 V vs SCE) upon potential reversal can be observed. As for **2** and **4**, the redox processes associated with the W centers are those of the lacunary POM precursor $[A\text{-}\alpha\text{-}SiW_9O_{34}]^{10-}$. Higher potentials see an ill-defined oxidation wave from −0.10 to 0.76 V versus SCE, which corresponds to the oxidation of Mn^{II} to Mn^{III}. The oxidation of Mn^{III} to Mn^{IV} peaks at 0.96 V versus SCE, which is slightly lower than it is for **2** (+1.02 vs SCE). The associated reduction of Mn^{IV} to Mn^{III} is located at 0.67 V versus SCE. In complete analogy with **2**, also **1** exhibits no observable decay when cycled between −1.0 V and +0.65 V versus SCE. This changes, however, when the higher vertex potential of the CV is increased to 1.15 V versus SCE. One of the occurring phenomena is that the W-reduction wave shifts to more negative potentials with increasing cycle number, as can be seen in Figure 9B. This indicates a kinetic hindrance of the otherwise facile reduction. Another observation is that the intensity of the anodic wave assigned to the oxidation of Mn^{IV} decreases in intensity with increasing cycle number. This indicates that, as for **2** and **4**, either **1** or its decomposition products are deposited onto the electrode. In contrast to the literature and **2** or **4**, however, in the case of **1** the electrode loses activity for the oxidation to Mn^{IV} upon successive cycling.[9d,h,l,26] Whether the thin film on the electrode has a different composition for **1** and **2** or **4** is an interesting question and should be investigated in the future. In CVs with a vertex potential of 1.5 V versus SCE an irreversible anodic wave can be observed for **1**, just as for **2** and **4** (Supporting Information, Figure S11). Figure S14 in the Supporting Information shows that the Mn^{IV} wave is followed by an irreversible oxidation at 1.4 V versus SCE, which is attributed to the Mn^{V} state.[9d,h,l,29] As for **2** and **4**, potential reversal at 1.5 V vs SCE leads to a significantly decreased Mn^{IV} reduction wave.

In conclusion, polyanion **1** can be clearly distinguished from **2** and **4**, which is attributed to the different oxidation states of the Mn centers. An in-depth electrochemical investigation of the presented manganese-containing tungstosilicates **1**−**5** is currently in preparation.

Magnetic Studies. The thermal variation of the $\chi_M T$ product for the Mn^{II}_3-containing polyanion **1** under an applied magnetic field of 0.1 T is shown in Figure 10. At room

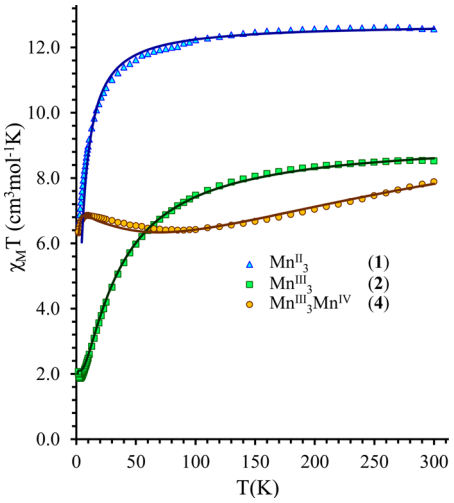

Figure 10. $\chi_M T$ vs T plots for the polyanion salts **1a**, **2a**, and **4a**. The solid lines correspond to simulations according to the Hamiltonians (eq 2−eq 4) with parameters described in the text.

temperature, the $\chi_M T$ product is 12.57 cm^3 K mol^{-1}, slightly lower than the expected value of 13.126 cm^3 K mol^{-1} for three noninteracting Mn^{II} ions ($S = 5/2$) with $g = 2$. Upon decreasing the temperature, the $\chi_M T$ product continuously decreases, reaching 6.85 cm^3 K mol^{-1} at 1.8 K, which further suggests antiferromagnetic interactions being operative in **1**. According to the single-crystal XRD analysis the magnetic core of **1** has C_3

dx.doi.org/10.1021/ic500425c | Inorg. Chem. 2014, 53, 5663−5673

symmetry. Hence the magnetic interaction can be described by an isotropic Hamiltonian, which defines the interaction between any two spins in an equilateral triangle.

$$H_t = -(2J_{12}S_1S_2 + 2J_{23}S_2S_3 + 2J_{13}S_1S_3) \quad \text{(eq 1)}$$

In the case of ferromagnetic interaction with $S_1 = S_2 = S_3$, the magnetic behavior can be described by only one coupling constant $J_{12} = J_{23} = J_{13} = J$. On the other hand, in the case of antiferromagnetic exchange interaction, the system is geometrically frustrated and cannot simultaneously satisfy all its pairwise exchange interactions; thus, the resulting ground state can have degeneracy. Under this condition, two exchange constants should be applied, to better characterize the magnetic interactions.[9g,31] A similar approach was used for different published examples of trinuclear, antiferromagnetically coupled clusters.[9g,17b,31,32]

Taking the structural information into consideration and the presence of dominant antiferromagnetic behavior in **1**, the general spin-Hamiltonian (eq 2) was applied to estimate the magnetic interaction between the three Mn^{II} centers.

$$H = -2J_a(S_1S_2 + S_2S_3) - 2J_bS_1S_3 \quad \text{(eq 2)}$$

where $S_1 = S_2 = S_3 = 5/2$. The exchange pathways in $Mn^{II}{}_3$ are shown in Figure 11.

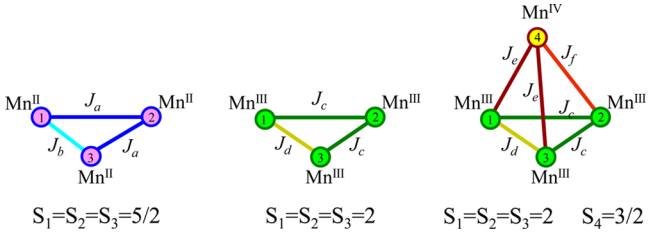

Figure 11. Exchange pathways within the manganese−oxo clusters in polyanions **1**, **2**, and **4**.

The best fit between theoretical, calculated, and experimental magnetic susceptibility was found for $J_a = -0.2$ cm^{-1}; $J_b = -0.3$ cm^{-1}; $g = 1.97$. The magnitude of the antiferromagnetic $J_{Mn(II)-Mn(II)}$ exchange coupling is similar to what was found for other Mn^{II}-containing heteropolytungstates.[9a,g,33] The fundamental spin state in **1** is $S = 1/2$, but the first excited magnetic level $S = 3/2$ is located at 0.2 cm^{-1}, and therefore at 1.8 K both spin states are populated (Supporting Information, Figure S15).

The $Mn^{III}{}_3$-containing polyanion **2** exibits also dominant antiferromagnetic behavior. The χ_MT product for **2** continuously decreases with temperature (at 0.1 T), see Figure 10. At room temperature, the χ_MT product is 8.61 cm^3 K mol^{-1}, lower than the expected value of 9.00 cm^3 K mol^{-1} for three noninteracting Mn^{III} ions ($S = 2$) with $g = 2$. Upon decreasing the temperature, the χ_MT product reaches 2.03 cm^3 K mol^{-1} at 1.8 K, suggesting the presence of antiferromagnetic interactions in **2**. Due to the structural similarities between polyanions **2** and **1**, a similar antiferromagnetic model was applied to estimate the magnetic interaction in **2**. Analyzing the magnetic data based on the isotropic general spin-Hamiltonian (eq 3), which contains two constants (J_c and J_d), we obtained the best fit with the experimental data at $J_c = -2.3$ cm^{-1}; $J_d = -1.2$ cm^{-1}; $g = 2.0$. The coupling constants for the Mn^{III}−Mn^{III} interactions are larger compared with those of Mn^{II}−Mn^{II} in a similar bridging arrangement, and are consistent with those reported previously.[9e,j] According to the energy diagram, at least three low-lying spin states are populated in **2**, $S = 1$ ($E_{s=1} = 0.0$ cm^{-1}); $S = 2$ ($E_{s=2} = 0.2$ cm^{-1}), and $S = 0$ ($E_{s=0} = 2.0$ cm^{-1}) at 2.0 K (Supporting Information, Figure S15).

$$H = -2J_c(S_1S_2 + S_2S_3) - 2J_dS_1S_3 \quad \text{(eq 3)}$$

For the $Mn^{III}{}_3Mn^{IV}$-containing polyanion **4** the value of χ_MT initially decreases with decreasing temperature from 7.82 cm^3 mol^{-1} K at room temperature to a minimum of 6.34 cm^3 K mol^{-1} at 77 K, then increases to 6.84 cm^3 K mol^{-1} at 8 K, and then decreases again, reaching 6.32 cm^3 K mol^{-1} at 1.8 K (Figure 10). The room temperature value for χ_MT is much lower than expected for three noninteracting Mn^{III} and one Mn^{IV} ion (9.00 + 1.875 cm^3 K mol^{-1}), suggesting the presence of significant antiferromagnetic interactions in **4**. According to the XRD data, polyanion **4** contains three Mn^{III} centers that are capped by a Mn^{IV} ion, located on the C_3 axis, leading to a mixed-valent $Mn^{III}{}_3Mn^{IV}O_3$ defective-cubane arrangement. Due to structural analogies, the magnetic interaction within the $Mn^{III}{}_3$ unit of $Mn^{III}{}_3Mn^{IV}$ in **4** should be very similar to polyanion **2**. As a result, the spin-Hamiltonian describing the isotropic exchange interactions can be written as

$$H = -2J_c(S_1S_2 + S_2S_3) - 2J_dS_1S_3 - 2J_e(S_1S_4 + S_3S_4) - 2J_fS_2S_4 \quad \text{(eq 4)}$$

The spin-Hamiltonian (eq 4) contains two supplementary coupling constants J_e and J_f to characterize the interaction between Mn^{III}−Mn^{IV}. The necessity for these two coupling constants is a result of the frustration phenomenon in the $Mn^{III}{}_3$ unit, which is propagated into the entire defective-cubane fragment.

The best match between the experimental and theoretical data was obtained for the set of parameters $J_c = -2.3$ cm^{-1}; $J_d = -1.2$ cm^{-1}; $J_e = -7.1$ cm^{-1}; $J_f = -35.2$ cm^{-1}; $g = 2.03$, where the first two correspond to the interaction between the Mn^{III} centers and is similar as in polyanion **2**. In the analysis of **4** we varied only the constants J_e and J_f, which reflect the interaction between the $Mn^{III}{}_3$ unit with Mn^{IV} ($S = 3/2$) and have a strong antiferromagnetic character, due to the presence of three supplementary carboxylate bridges between the Mn^{III}−Mn^{IV} ions. The small deviations between the theoretical and experimental data in the temperature dependence of χ_MT can be rationalized by the presence of zero-field splitting (ZFS) parameters, which are neglected in these simulations. The distribution of spin states for polyanion **4** is presented in Supporting Information, Figure S15. The three spin states $S = 5/2$ ($E_{=5/2} = 0$ cm^{-1}), $S = 7/2$ ($E_{=7/2} = 0.37$ cm^{-1}), and $S = 3/2$ ($E_{=3/2} = 1.05$ cm^{-1}) are predominantly populated at low temperature. The increase of χ_MT at low temperature (70−10 K, see Figure 10) corresponds to a temperature-dependent population redistribution between different spin states. A similar increase of χ_MT at low temperature in a completely antiferromagnetically coupled system of C_3 symmetry in metal−oxo clusters has rarely been reported.[34]

The alternating current magnetic susceptibility was measured at zero and 2000 Oe direct magnetic fields for polyanions **1**, **2**, and **4**. No signal or frequency-dependence was detected, in contrast to a reported $Mn^{III}{}_4Mn^{II}{}_2$-containing polyanion.[9e] This can be explained by the presence of a population redistribution of the different spin states in **2** and **4**, and/or also by positive ZFS parameters. The estimation of ZFS from the magnetization data (Supporting Information, Figure S16) under the condition

dx.doi.org/10.1021/ic500425c | Inorg. Chem. 2014, 53, 5663−5673

of simultaneous population of different spin states associated with relatively small exchange parameters is difficult and results in ill-defined parameters for ZFS with a large uncertainty.

CONCLUSIONS

In conclusion, the five manganese-containing tungstosilicates, namely, $[Mn^{II}_3(OH)_3(H_2O)_3(A\text{-}\alpha\text{-}SiW_9O_{34})]^{7-}$ (**1**), $[Mn^{III}_3(OH)_3(H_2O)_3(A\text{-}\alpha\text{-}SiW_9O_{34})]^{4-}$ (**2**), $[Mn^{III}_3(OH)_3(H_2O)_3(A\text{-}\beta\text{-}SiW_9O_{34})]^{4-}$ (**3**), $[Mn^{III}_3Mn^{IV}O_3(CH_3COO)_3(A\text{-}\alpha\text{-}SiW_9O_{34})]^{6-}$ (**4**), and $[Mn^{III}_3Mn^{IV}O_3(CH_3COO)_3(A\text{-}\beta\text{-}SiW_9O_{34})]^{6-}$ (**5**), were successfully synthesized in aqueous media. Their isolated salts **1a**, **2a**, **3a**, **4a**, and **5a** were fully characterized in the solid state by single-crystal XRD, IR spectroscopy, and TGA. The compounds **1a**, **2a**, and **4a** were investigated in the solid state by magnetic studies and in solution by electrochemistry. Our work demonstrates a novel reactive feature of $\mathbf{Mn_{12}}$ with lacunary polyanions and also reemphasizes that POMs can stabilize high-valent manganese. The electrochemical study demonstrates that polyanions **1**, **2**, and **4** are stable in solution and that the $Mn^{II/III}$ centers can be oxidized and reduced without decomposition of the polyanion. These features render our Mn-containing POMs highly interesting for redox-directed catalysis reactions. Moreover, the magnetic investigation exhibited the presence of dominant antiferromagnetic behavior in polyanions **1**, **2**, and **4**. The relative magnitude of the antiferromagnetic interactions is $J_{MnII-MnII} < J_{MnIII-MnIII} < J_{MnIII-MnIV}$.

ASSOCIATED CONTENT

Supporting Information

Table S1 (crystallographic data), Figures S1−S3 (representative synthesis schemes), Figures S4−S8 (thermograms), Figure S9 (rotational isomers), Tables S2, S3, and S4 (selected bond lengths and bond valence sums), Figures S10−S14 (electrochemical studies), and Figures S15−S16 (magnetic studies). This material is available free of charge via the Internet at http://pubs.acs.org

AUTHOR INFORMATION

Corresponding Author

*E-mail: u.kortz@jacobs-university.de. Fax: (+49) 421-200-3229. Homepage: www.jacobs-university.de/ses/ukortz.

Present Address

▽Institute of Nanotechnology, Karlsruhe Institute of Technology, P.O. Box 3640, 76021 Karlsruhe, Germany.

Notes

The authors declare no competing financial interest.

ACKNOWLEDGMENTS

U.K. thanks Jacobs University and the German Science Foundation (DFG KO-2288/20-1) for research support and the EU-COST D40 Action, where this work was presented as a poster entitled "Multinuclear Manganese-Containing Polyoxotungstates: Synthesis, Structure and Catalytic Potential" at the COST D40 meeting in Valletta, Malta on 14−16 June 2011. R.A. thanks DAAD (Deutscher Akademischer Austauschdienst) for a doctoral fellowship to pursue his Ph.D. studies at Jacobs University, Germany. U.K. also acknowledges the COST Action CM1203 (PoCheMoN). We thank Prof. Geoffrey B. Jameson (Massey University, New Zealand) for valuable comments, and Mr. Ali Haider for performing some TGA measurements. Figures 1, 3, 5, 7, S1, S2, S3, and S9 were generated by Diamond Version 3.2 (copyright Crystal Impact GbR).

REFERENCES

(1) (a) Pope, M. T. *Heteropoly and Isopoly Oxometalates;* Springer-Verlag: Berlin, Germany, 1983. (b) Pope, M. T.; Müller, A. *Polyoxometalate Chemistry From Topology via Self-Assembly to Applications;* Kluwer Academic Publishers: Dordrecht, Netherlands, 2001. (c) *Eur. J. Inorg. Chem.* **2009**, Kortz, U., Ed.; 5055−5276. (d) Pope, M. T.; Kortz, U., Polyoxometalates. In *Encyclopedia of Inorganic and Bioinorganic Chemistry;* John Wiley & Sons, Ltd: Hoboken, NJ, 2012.

(2) (a) Bonchio, M.; Carraro, M.; Scorrano, G.; Kortz, U. *Adv. Synth. Catal.* **2005**, *347*, 1909−1912. (b) Bonchio, M.; Carraro, M.; Sartorel, A.; Scorrano, G.; Kortz, U. *J. Mol. Catal. A: Chem.* **2006**, *251*, 93−99. (c) Bonchio, M.; Carraro, M.; Farinazzo, A.; Sartorel, A.; Scorrano, G.; Kortz, U. *J. Mol. Catal. A: Chem.* **2007**, *262*, 36−40. (d) Hussain, F.; Bassil, B. S.; Kortz, U.; Kholdeeva, O. A.; Timofeeva, M. N.; de Oliveira, P.; Keita, B.; Nadjo, L. *Chem.—Eur. J.* **2007**, *13*, 4733−4742. (e) Carraro, M.; Sartorel, A.; Scorrano, G.; Maccato, C.; Dickman, M. H.; Kortz, U.; Bonchio, M. *Angew. Chem., Int. Ed.* **2008**, *47*, 7275−7279. (f) Kholdeeva, O. A.; Donoeva, B. G.; Trubitsina, T. A.; Al-Kadamany, G.; Kortz, U. *Eur. J. Inorg. Chem.* **2009**, 5134−5141. (g) Bonchio, M.; Carraro, M.; Sartorel, A.; Maccato, C.; Scorrano, G.; Dickman, M. H.; Kortz, U. *Abstr. Pap., Jt. Conf.—Chem. Inst. Can. Am. Chem. Soc.* **2009**, 237. (h) Sartorel, A.; Carraro, M.; Scorrano, G.; Bassil, B. S.; Dickman, M. H.; Keita, B.; Nadjo, L.; Kortz, U.; Bonchio, M. *Chem.—Eur. J.* **2009**, *15*, 7854−7858. (i) Al-Kadamany, G.; Mal, S. S.; Milev, B.; Donoeva, B. G.; Maksimovskaya, R. I.; Kholdeeva, O. A.; Kortz, U. *Chem.—Eur. J.* **2010**, *16*, 11797−11800. (j) Antonova, N. S.; Carbo, J. J.; Kortz, U.; Kholdeeva, O. A.; Poblet, J. M. *J. Am. Chem. Soc.* **2010**, *132*, 7488−7497. (k) Donoeva, B. G.; Trubitsina, T. A.; Antonova, N. S.; Carbo, J. J.; Poblet, J. M.; Al-Kadamany, G.; Kortz, U.; Kholdeeva, O. A. *Eur. J. Inorg. Chem.* **2010**, 5312−5317. (l) Donoeva, B. G.; Trubitsyna, T. A.; Al-Kadamany, G.; Kortz, U.; Kholdeeva, O. A. *Kinet. Catal.* **2010**, *51*, 816−822. (m) Mal, S. S.; Nsouli, N. H.; Carraro, M.; Sartorel, A.; Scorrano, G.; Oelrich, H.; Walder, L.; Bonchio, M.; Kortz, U. *Inorg. Chem.* **2010**, *49*, 7−9. (n) Carraro, M.; Nsouli, N.; Oelrich, H.; Sartorel, A.; Soraru, A.; Mal, S. S.; Scorrano, G.; Walder, L.; Kortz, U.; Bonchio, M. *Chem.—Eur. J.* **2011**, *17*, 8371−8378. (o) Al-Oweini, R.; Aghyarian, S.; El-Rassy, H. *J. Sol-Gel Sci. Technol.* **2012**, *61*, 541−550. (p) Nsouli, N. H.; Chubarova, E. V.; Al-Oweini, R.; Bassil, B. S.; Sadakane, M.; Kortz, U. *Eur. J. Inorg. Chem.* **2013**, 1742−1747.

(3) Ibrahim, M.; Lan, Y. H.; Bassil, B. S.; Xiang, Y. X.; Suchopar, A.; Powell, A. K.; Kortz, U. *Angew. Chem., Int. Ed.* **2011**, *50*, 4708−4711.

(4) (a) Reinoso, S.; Dickman, M. H.; Praetorius, A.; Piedra-Garza, L. F.; Kortz, U. *Inorg. Chem.* **2008**, *47*, 8798−8806. (b) Ball, V.; Bernsmann, F.; Werner, S.; Voegel, J. C.; Piedra-Garza, L. F.; Kortz, U. *Eur. J. Inorg. Chem.* **2009**, 5115−5124. (c) Piedra-Garza, L. F.; Reinoso, S.; Dickman, M. H.; Sanguineti, M. M.; Kortz, U. *Dalton Trans.* **2009**, 6231−6234. (d) Breunig, H. J.; Koehne, T.; Moldovan, O.; Preda, A. M.; Silvestru, A.; Silvestru, C.; Varga, R. A.; Piedra-Garza, L. F.; Kortz, U. *J. Organomet. Chem.* **2010**, *695*, 1307−1313. (e) Reinoso, S.; Piedra-Garza, L. F.; Dickman, M. H.; Praetorius, A.; Biesemans, M.; Willem, R.; Kortz, U. *Dalton Trans.* **2010**, *39*, 248−255. (f) Piedra-Garza, L.; Barsukova-Stuckart, M.; Bassil, B.; Al-Oweini, R.; Kortz, U. *J. Cluster Sci.* **2012**, *23*, 939−951.

(5) (a) Kortz, U.; Marquer, C.; Thouvenot, R.; Nierlich, M. *Inorg. Chem.* **2003**, *42*, 1158−1162. (b) Kortz, U.; Vaissermann, J.; Thouvenot, R.; Gouzerh, P. *Inorg. Chem.* **2003**, *42*, 1135−1139. (c) Chubarova, E. V.; Klöck, C.; Dickman, M. H.; Kortz, U. *J. Cluster Sci.* **2007**, *18*, 697−710.

(6) (a) Vilà-Nadal, L.; Rodríguez-Fortea, A.; Yan, L.-K.; Wilson, E. F.; Cronin, L.; Poblet, J. M. *Angew. Chem., Int. Ed.* **2009**, *48*, 5452−5456. (b) Vilà-Nadal, L.; Mitchell, S. G.; Rodríguez-Fortea, A.; Miras, H. N.; Cronin, L.; Poblet, J. M. *Phys. Chem. Chem. Phys.* **2011**, *13*, 20136−20145.

(7) (a) Yamase, T.; Pope, M. T. *Polyoxometalate chemistry for nano-composite design;* Kluwer Academic/Plenum Publishers: New York, 2002; p viii, 235. (b) Kortz, U.; Müller, A.; van Slageren, J.; Schnack, J.; Dalal, N. S.; Dressel, M. *Coord. Chem. Rev.* **2009**, *253*, 2315−2327.
(8) (a) Kortz, U.; Al-Kassem, N. K.; Savelieff, M. G.; Al Kadi, N. A.; Sadakane, M. *Inorg. Chem.* **2001**, *40*, 4742−4749. (b) Kortz, U.; Nellutla, S.; Stowe, A. C.; Dalal, N. S.; Rauwald, U.; Danquah, W.; Ravot, D. *Inorg. Chem.* **2004**, *43*, 2308−2317. (c) Bassil, B. S.; Ibrahim, M.; Al-Oweini, R.; Asano, M.; Wang, Z. X.; van Tol, J.; Dalal, N. S.; Choi, K. Y.; Biboum, R. N.; Keita, B.; Nadjo, L.; Kortz, U. *Angew. Chem., Int. Ed.* **2011**, *50*, 5961−5964. (d) Kortz, U.; Savelieff, M. G.; Bassil, B. S.; Keita, B.; Nadjo, L. *Inorg. Chem.* **2002**, *41*, 783−789. (e) Kortz, U.; Nellutla, S.; Stowe, A. C.; Dalal, N. S.; van Tol, J.; Bassil, B. S. *Inorg. Chem.* **2004**, *43*, 144−154. (f) Bi, L. H.; Kortz, U.; Nellutla, S.; Stowe, A. C.; van Tol, J.; Dalal, N. S.; Keita, B.; Nadjo, L. *Inorg. Chem.* **2005**, *44*, 896−903. (g) Zheng, S.-T.; Yang, G.-Y. *Chem. Soc. Rev.* **2012**, *41*, 7623−7646. (h) Oms, O.; Dolbecq, A.; Mialane, P. *Chem. Soc. Rev.* **2012**, *41*, 7497−7536.
(9) (a) Kortz, U.; Isber, S.; Dickman, M. H.; Ravot, D. *Inorg. Chem.* **2000**, *39*, 2915−2922. (b) Kortz, U.; Matta, S. *Inorg. Chem.* **2001**, *40*, 815−817. (c) Mbomekalle, I. M.; Keita, B.; Nierlich, M.; Kortz, U.; Berthet, P.; Nadjo, L. *Inorg. Chem.* **2003**, *42*, 5143−5152. (d) Bassil, B. S.; Dickman, M. H.; Reicke, M.; Kortz, U.; Keita, B.; Nadjo, L. *Dalton Trans.* **2006**, 4253−4259. (e) Ritchie, C.; Ferguson, A.; Nojiri, H.; Miras, H. N.; Song, Y. F.; Long, D. L.; Burkholder, E.; Murrie, M.; Kögerler, P.; Brechin, E. K.; Cronin, L. *Angew. Chem., Int. Ed.* **2008**, *47*, 5609−5612. (f) Song, Y. F.; Long, D. L.; Kelly, S. E.; Cronin, L. *Inorg. Chem.* **2008**, *47*, 9137−9139. (g) Nsouli, N. H.; Ismail, A. H.; Helgadottir, I. S.; Dickman, M. H.; Clemente-Juan, J. M.; Kortz, U. *Inorg. Chem.* **2009**, *48*, 5884−5890. (h) Bassil, B. S.; Ibrahim, M.; Mal, S. S.; Suchopar, A.; Biboum, R. N.; Keita, B.; Nadjo, L.; Nellutla, S.; van Tol, J.; Dalal, N. S.; Kortz, U. *Inorg. Chem.* **2010**, *49*, 4949−4959. (i) Mitchell, S. G.; Miras, H. N.; Long, D. L.; Cronin, L. *Inorg. Chim. Acta* **2010**, *363*, 4240−4246. (j) Dutta, D.; Jana, A. D.; Debnath, M.; Mostafa, G.; Clérac, R.; Tojal, J. G.; Ali, M. *Eur. J. Inorg. Chem.* **2010**, *2010*, 5517−5522. (k) Mitchell, S. G.; Boyd, T.; Miras, H. N.; Long, D. L.; Cronin, L. *Inorg. Chem.* **2011**, *50*, 136−143. (l) Al-Oweini, R.; Bassil, B. S.; Palden, T.; Keita, B.; Lan, Y.; Powell, A. K.; Kortz, U. *Polyhedron* **2013**, *52*, 461−466.
(10) (a) Fang, X. K.; Kögerler, P. *Angew. Chem., Int. Ed.* **2008**, *47*, 8123−8126. (b) Fang, X. K.; Kögerler, P. *Chem. Commun.* **2008**, 3396−3398. (c) Wu, Q.; Li, Y.-G.; Wang, Y.-H.; Wang, E.-B.; Zhang, Z.-M.; Clérac, R. *Inorg. Chem.* **2009**, *48*, 1606−1612. (d) Fang, X. K.; Speldrich, M.; Schilder, H.; Cao, R.; O'Halloran, K. P.; Hill, C. L.; Kögerler, P. *Chem. Commun.* **2010**, *46*, 2760−2765. (e) Fang, X.; Kögerler, P.; Furukawa, Y.; Speldrich, M.; Luban, M. *Angew. Chem., Int. Ed.* **2011**, *50*, 5212−5216.
(11) Lis, T. *Acta Crystallogr., Sect. B: Struct. Sci.* **1980**, *36*, 2042−2046.
(12) Sessoli, R.; Gatteschi, D.; Caneschi, A.; Novak, M. A. *Nature* **1993**, *365*, 141−143.
(13) (a) Hervé, G.; Tézé, A. *Inorg. Chem.* **1977**, *16*, 2115−2117. (b) Laronze, N.; Marrot, J.; Hervé, G. *Inorg. Chem.* **2003**, *42*, 5857−5862. (c) Téazé, A.; Hervé, G.; Finke, R. G.; Lyon, D. K., α-, β-, and γ-Dodecatungstosilicic Acids: Isomers and Related Lacunary Compounds. In *Inorganic Synthesis;* John Wiley & Sons, Inc.: Hoboken, NJ, 2007; pp 85−96.
(14) *SAINT;* Bruker AXS Inc.: Madison, WI, 2007.
(15) Sheldrick, G. M. *Acta Crystallogr., Sect. A: Found. Crystallogr.* **2008**, *64*, 112−122.
(16) Mal, S. S.; Bassil, B. S.; Ibrahim, M.; Nellutla, S.; van Tol, J.; Dalal, N. S.; Fernández, J. A.; López, X.; Poblet, J. M.; Biboum, R. N.; Kelta, B.; Kortz, U. *Inorg. Chem.* **2009**, *48*, 11636−11645.
(17) (a) Pascal, P. *Ann. Chim. Phys.* **1910**, *19*, 5. (b) Kahn, O. *Molecular Magnetism;* VCH Publishers, Inc.: New York, Weinheim, Cambridge, 1993.
(18) Borras-Almenar, J. J.; Clemente-Juan, J. M.; Coronado, E.; Tsukerblat, B. S. *J. Comput. Chem.* **2001**, *22*, 985−991.
(19) Brown, I. D.; Altermatt, D. *Acta Crystallogr., Sect. B: Struct. Sci.* **1985**, *41*, 244−247.
(20) Liu, J. G.; Ortéga, F.; Sethuraman, P.; Katsoulis, D. E.; Costello, C. E.; Pope, M. T. *J. Chem. Soc., Dalton Trans.* **1992**, 1901−1906.
(21) Shevchenko, D.; Huang, P.; Bon, V. V.; Anderlund, M. F.; Kokozay, V. N.; Styring, S.; Thapper, A. *Dalton Trans.* **2013**, *42*, 5130−5139.
(22) (a) Wang, S.; Tsai, H.-L.; Libby, E.; Folting, K.; Streib, W. E.; Hendrickson, D. N.; Christou, G. *Inorg. Chem.* **1996**, *35*, 7578−7589. (b) Hendrickson, D. N.; Christou, G.; Schmitt, E. A.; Libby, E.; Bashkin, J. S.; Wang, S.; Tsai, H. L.; Vincent, J. B.; Boyd, P. D. W. *J. Am. Chem. Soc.* **1992**, *114*, 2455−2471. (c) Li, Q.; Vincent, J. B.; Libby, E.; Chang, H.-R.; Huffman, J. C.; Boyd, P. D. W.; Christou, G.; Hendrickson, D. N. *Angew. Chem., Int. Ed.* **1988**, *27*, 1731−1733.
(23) San Felices, L.; Vitoria, P.; Gutiérrez-Zorrilla, J. M.; Lezama, L.; Reinoso, S. *Inorg. Chem.* **2006**, *45*, 7748−7757.
(24) (a) Thouvenot, R.; Fournier, M.; Franck, R.; Rocchiccioli-Deltcheff, C. *Inorg. Chem.* **1984**, *23*, 598−605. (b) Bridgeman, A. J. *Chem. Phys.* **2003**, *287*, 55−69. (c) Al-Oweini, R.; El-Rassy, H. *J. Mol. Struct.* **2009**, *919*, 140−145.
(25) (a) Zhang, X. Y.; Pope, M. T.; Chance, M. R.; Jameson, G. B. *Polyhedron* **1995**, *14*, 1381−1392. (b) Zhang, X. Y.; Jameson, G. B.; O'Connor, C. J.; Pope, M. T. *Polyhedron* **1996**, *15*, 917−922. (c) Zhang, X. Y.; O'Connor, C. J.; Jameson, G. B.; Pope, M. T. *Inorg. Chem.* **1996**, *35*, 30−34.
(26) Keita, B.; Mialane, P.; Sécheresse, F.; de Oliveira, P.; Nadjo, L. *Electrochem. Commun.* **2007**, *9*, 164−172.
(27) Ammam, M.; Keita, B.; Nadjo, L.; Mbomekalle, I. M.; Ritorto, M. D.; Anderson, T. M.; Neiwert, W. A.; Hill, C. L.; Fransaer, J. *Electroanalysis* **2011**, *23*, 1427−1434.
(28) Pichon, C.; Mialane, P.; Dolbecq, A.; Marrot, J.; Rivière, E.; Bassil, B. S.; Kortz, U.; Keita, B.; Nadjo, L.; Sécheresse, F. *Inorg. Chem.* **2008**, *47*, 11120−11128.
(29) Sadakane, M.; Steckhan, E. *Acta Chem. Scand.* **1999**, *53*, 837−841.
(30) Keita, B.; Nadjo, L. Electrochemistry of Isopoly and Heteropoly Oxometalates. In *Encyclopedia of Electrochemistry;* Bard, A. J.; Stratmann, M., Eds. Wiley-VCH: Weinheim, Germany, 2006; Vol. 7.
(31) (a) Jayasooriya, U. A.; Cannon, R. D.; White, R. P.; Stride, J. A.; Grinter, R.; Kearley, G. J. *J. Chem. Phys.* **1993**, *98*, 9303−9310. (b) Cannon, R. D.; Jayasooriya, U. A.; Wu, R.; arapKoske, S. K.; Stride, J. A.; Nielsen, O. F.; White, R. P.; Kearley, G. J.; Summerfield, D. *J. Am. Chem. Soc.* **1994**, *116*, 11869−11874. (c) Long, G. J.; Robinson, W. T.; Tappmeyer, W. P.; Bridges, D. L. *J. Chem. Soc., Dalton Trans.* **1973**, 573−579. (d) Castro, S. L.; Streib, W. E.; Sun, J.-S.; Christou, G. *Inorg. Chem.* **1996**, *35*, 4462−4468.
(32) (a) Kahn, O. *Struct. Bonding (Berlin)* **1987**, *68*, 89−167. (b) Kambe, K. *J. Phys. Soc. Jpn.* **1950**, *5*, 48−51. (c) Dziobkowski, C. T.; Wrobleski, J. T.; Brown, D. B. *Inorg. Chem.* **1981**, *20*, 679−684. (d) Prodius, D.; Macaev, F.; Stingaci, E.; Pogrebnoi, V.; Mereacre, V.; Novitchi, G.; Kostakis, G. E.; Anson, C. E.; Powell, A. K. *Chem. Commun.* **2013**, *49*, 1915−1917. (e) Novitchi, G.; Helm, L.; Anson, C.; Powell, A. K.; Merbach, A. E. *Inorg. Chem.* **2011**, *50*, 10402−10416. (f) Tsukerblat, B. S.; Kuyavskaya, B. Y.; Belinskii, M. I.; Ablov, A. V.; Novotortsev, V. M.; Kalinnikov, V. T. *Theor. Chim. Acta* **1975**, *38*, 131−138.
(33) Gomez-Garcia, C. J.; Coronado, E.; Gomez-Romero, P.; Casan-Pastor, N. *Inorg. Chem.* **1993**, *32*, 3378−3381.
(34) (a) Guedel, H. U.; Hauser, U. *Inorg. Chem.* **1980**, *19*, 1325−1328. (b) Batchelor, L. J.; Sander, M.; Tuna, F.; Helliwell, M.; Moro, F.; van Slageren, J.; Burzuri, E.; Montero, O.; Evangelisti, M.; Luis, F.; McInnes, E. J. L. *Dalton Trans.* **2011**, *40*, 5278−5284. (c) Pavlishchuk, V.; Birkelbach, F.; Weyhermüller, T.; Wieghardt, K.; Chaudhuri, P. *Inorg. Chem.* **2002**, *41*, 4405−4416. (d) Accorsi, S.; Barra, A.-L.; Caneschi, A.; Chastanet, G.; Cornia, A.; Fabretti, A. C.; Gatteschi, D.; Mortalò, C.; Olivieri, E.; Parenti, F.; Rosa, P.; Sessoli, R.; Sorace, L.; Wernsdorfer, W.; Zobbi, L. *J. Am. Chem. Soc.* **2006**, *128*, 4742−4755.
(35) Cowan, J. J.; Bailey, A. J.; Heintz, R. A.; Do, B. T.; Hardeastle, K. I.; Hill, C. L.; Weinstock, I. A. *Inorg. Chem.* **2001**, *40*, 6666−6675.
(36) Khenkin, A. M.; Kumar, D.; Shaik, S.; Neumann, R. *J. Am. Chem. Soc.* **2006**, *128*, 15451−15460.

(37) Car, P. E.; Spingler, B.; Weyeneth, S.; Patscheider, J.; Patzke, G. R. *Polyhedron* **2013**, *52*, 151−158.
(38) Zhao, Z. F.; Zhou, B. B.; Zheng, S. T.; Su, Z. H.; Wang, C. M. *Inorg. Chim. Acta* **2009**, *362*, 5038−5042.
(39) Botar, B.; Geletii, Y. V.; Kogerler, P.; Musaev, D. G.; Morokuma, K.; Weinstock, I. A.; Hill, C. L. *Dalton Trans.* **2005**, 2017−2021.
(40) Mialane, P.; Marrot, J.; Rivière, E.; Nebout, J.; Hervé, G. *Inorg. Chem.* **2001**, *40*, 44−48.
(41) Gomez-Garcia, C. J.; Borras-Almenar, J. J.; Coronado, E.; Ouahab, L. *Inorg. Chem.* **1994**, *33*, 4016−4022.
(42) Mialane, P.; Duboc, C.; Marrot, J.; Riviere, E.; Dolbecq, A.; Secheresse, F. *Chem.—Eur. J.* **2006**, *12*, 1950−1959.
(43) Mitchell, S. G.; Khanra, S.; Miras, H. N.; Boyd, T.; Long, D. L.; Cronin, L. *Chem. Commun.* **2009**, 2712−2714.
(44) Jiang, N.; Li, F. Y.; Xu, L.; Li, Y. G.; Li, J. M. *Inorg. Chem. Commun.* **2010**, *13*, 372−375.
(45) Mitchell, S. G.; Molina, P. I.; Khanra, S.; Miras, H. N.; Prescimone, A.; Cooper, G. J. T.; Winter, R. S.; Brechin, E. K.; Long, D. L.; Cogdell, R. J.; Cronin, L. *Angew. Chem., Int. Ed.* **2011**, *50*, 9154−9157.
(46) Chen, L. J.; Shi, D. Y.; Zhao, J. W.; Wang, Y. L.; Ma, P. T.; Wang, J. P.; Niu, J. Y. *Cryst. Growth Des.* **2011**, *11*, 1913−1923.
(47) Fang, X. K.; Kögerler, P.; Speldrich, M.; Schilder, H.; Luban, M. *Chem. Commun.* **2012**, *48*, 1218−1220.
(48) Fang, X. K.; Luban, M. *Chem. Commun.* **2011**, *47*, 3066−3068.